Influence of Cellulosic Additives on Tricalcium Silicate Hydration: Nuclear Magnetic Resonance Relaxation Time Analysis

Marcella Alesiani,[‡] Silvia Capuani,[‡] Rodorico Giorgi,[†] Bruno Maraviglia,[‡] Ilaria Pirazzoli,[‡] Francesca Ridi,[†] and Piero Baglioni*[,†]

Department of Chemistry and CSGI, University of Florence, via della Lastruccia 3, Sesto Fiorentino, 50019 Florence, Italy, and Department of Physics, 'La Sapienza' University and INFM UdR Roma1, P.le A. Moro 5, Rome, Italy

Received: December 16, 2003; In Final Form: February 4, 2004

This paper reports a study on the effects of cellulose additives on the setting process of tricalcium silicate (C_3S) paste. Cellulose and cellulose derivatives are largely used in the cement industry due to their excellent water carrying capacity that makes these additives essential in the practice of the extrusion processes. However, how they are effective in many processes is not known. We addressed this point investigating the hydration kinetics of C_3S in the presence of cellulose derivative by thermal analysis and water proton NMR relaxation. Both these methods provided useful information on the mechanisms of the C_3S curing process involving cellulose. The experimental results clearly show that cellulose additives act as a regulator of water release during the whole hydration process. A quantitative description of this process is reported.

Introduction

Cement is one of the most important materials in human activity. The development of its mechanical properties is the result of the reaction of water with the cement components. The hydration process produces the so-called CSH gel, characterized by an intricate structure with low porosity and formed of irregular interlocking fibers growing from the surfaces of the grains.[1,2] Several additives have been formulated in order to produce cements with better performances (fluidizers, plasticizers, etc.). Among them, cellulose additives have been recently investigated since they consistently improve some features of cement, allowing cement extrusion and opening new perspectives for cement applications.[3−9] Extrusion is a processing technique that confers high performance characteristics to cement materials. It is a "forming" process in which a highly viscous and plastic-like mixture is forced trough a die, a rigid open of desired cross-section. Two conflicting requirements make this process of difficult application: the paste should be fluid enough to allow the mixing and thrusting through the die, and the extruded specimen should be stiff enough to allow the easy handling without any shape variation. These two requirements are fulfilled by the addition of polymeric derivatives of cellulose to the paste. Nowadays, there is a growing interest in the use of extrusion processes, as, for example, in the fiber-reinforced cement composites industry.

Despite the evident importance of such knowledge for the extrusion technique development, cellulose compounds interaction with cement, and their contributions to the hydration reaction are far from being clarified, which is a challenge for physicists and chemists.[3,4] Moreover, the hydration mechanism and the hardening of cement paste are not fully understood. In previous studies we contribute to knowledge of the hydration mechanism mainly using quasi-elastic neutron scattering (QENS) and differential scanning calorimetry (DSC).[10−19] For the first time we proposed a new DSC method to asses a scale of additive "performance" based on the activation energies involved in nucleation processes present in the cement setting and hardening.[11,19] During these processes the porous characteristics change as a function of time. In this view, the study of porous characteristics of cement pastes is particularly relevant in order to evaluate the structural modifications induced by additives.

The almost unique technique used to obtain information about the pore structure of a hardened cement paste is mercury intrusion porosimetry (MIP). Some criticisms about the application of this technique to the study of cement characteristics have been raised.[20−22] MIP allows investigation of hardened structures, at very long curing times, when variation in pore structure can no longer occur. On the other hand, the evolution of the pore size distribution in the early stages of hydration is poorly known.

This study is aimed at investigation both of the mechanism of action of cellulose polymers and of the pore structure evolution during the C_3S phase hydration process. In particular, the longitudinal and the transverse magnetization relaxation of the water proton and the role of methyl hydroxyethyl cellulose (MHEC) in the C_3S paste hydration have been investigated.

Several papers have been published on this subject by using NMR relaxation.[23,24] ^{1}H NMR offers a number of advantages: (i) nondestructive testing; (ii) no complex preparation procedure is required (e.g., drying) that could produce microstructure changes (e.g., pore collapse); (iii) water constituting the paste is directly probed, thus no liquid or gas intrusion is needed. Liquid water is usually used as contrast agent for monitoring the pore structure modifications of the hydrating cement paste.

The estimation of pore-size distributions is of considerable importance in the development of models to describe the behavior of fluids confined within porous media. NMR spin−lattice relaxation measurements of confined fluids are sensitive to both the pore size and geometry.[25−28] The correlation between

* Corresponding author. Phone: +39 055 4573033. Fax: +39 055 4573032. E-mail: baglioni@csgi.unifi.it.
[†] University of Florence
[‡] 'La Sapienza' University and INFM UdR Roma1.

10.1021/jp037876n CCC: $27.50
Published on Web 03/23/2004

the pore dimensions in water-saturated porous media and the relaxation time values has been widely discussed in a number of papers.[29−32] Measurements of the ^{1}H NMR spin−lattice and spin−spin relaxation time have been demonstrated as important tools in the characterization of pore size distribution of various porous materials.[33−35]

*T*1 values have been successfully used to estimate the permeability, the wettability and the fluid saturation.[36,37] *T*2 measurements have also been proved to be highly correlated to the surface area and pore size distribution.[33] Pore size distributions (PSDs) for the early stage of hydration have been obtained from spin−lattice relaxation rates, directly processed for obtaining PSDs[33,34] according to the Brownstein and Tarr model[38] (see also appendix), based on the classical approach of the magnetization diffusion elaborated by Bloch and Torrey.[39]

Differential scanning calorimetry has been employed to follow the whole hydration process, according to the procedure described in previous papers.[11,19]

Synthetic tricalcium silicate (C_3S) has been chosen due to its phase abundance in typical Portland cement (from 70% to 80%) and its importance in affecting the cement paste characteristics, such as setting time and hardening behavior.

Experimental Section

Tricalcium silicate (C_3S) has been synthesized by CTG-Italcementi Group. The powder had a BET specific surface area of 0.40 ± 0.05 m^2/g and particle median diameter of 11.5 μm. Water was purified by a Millipore Organex system ($R > 18$ MΩ cm). Methyl-hydroxy-ethyl cellulose, MHEC, was obtained from Bayer (commercial name Walocel MKX PP 0.1 with a DS = 1.75 (CH_3) and MS = 2 (CH_2CH_2OH) −OH substitution degree, and a 40 000 average molecular weight). Samples for NMR experiments were prepared with prehydrated cellulose (3.6% w/w in water). Hydrated cellulose gel, 150 mg, was mixed with 2 g of C_3S and 655.4 mg of water. The final concentration was 0.4% water/C_3S w/w and 0.27% MHEC on C_3S by weight. The paste was manually mixed for about 1 min onto a glass surface: 1 g of this paste was then transferred in a Teflon vial and sealed with Parafilm.

The NMR experimental measurements were performed with a Bruker Biospec BMT 70/15 equipped with AVANCE digital spectrometer. A superconducting horizontal magnet generating a 7.05 T static field H_0 in a cylindrical region, 20 cm in length and 15 cm in diameter, was employed. A birdcage radio frequency coil of 15-cm diameter and 60-cm length and tuned to 300 MHz for the ^{1}H resonance was used to irradiate samples. The sample container consists of a cylindrical volume with diameter of 6 cm and length of 6 cm.

Proton spin−lattice (T1) relaxation times were determined by using an inversion recovery (IR) sequence.[40] A 180° radio frequency pulse was applied for the inversion of the whole magnetization, followed by a 90° pulse for signal detection.

Modern NMR measuring tools primarily use the CPMG (Carr-Purcell-Meiboom-Gill) multipulse technique to obtain transverse relaxation data. *T*2 relaxation time values were thus acquired by a standard CPMG pulse sequence.[40] All experiments have been performed at room temperature (20 °C).

According to the Brownstein and Tarr model, pore geometry and NMR relaxation intensity are correlated by the coefficients of a sum of normal modes that depend on the diffusion coefficient *D*, on the surface-to-volume ratio, and on the pore size *r*. Basic assumptions for the model validity are the following: (i) bulk fluid intrinsic relaxation; (ii) surface relaxation for the fluid layers in contact with the pore walls; (iii) paramagnetic impurities acting as relaxation sinks; (iv) diffusion within the pore space with the coefficient *D*, assumed as the bulk water autodiffusion coefficient. Independently of the pore geometry, solutions were evaluated under the hypothesis that the effect on the relaxation due to the fluid interaction with the pore surface is uniform and quantifiable with the ρ parameter.[41,42]

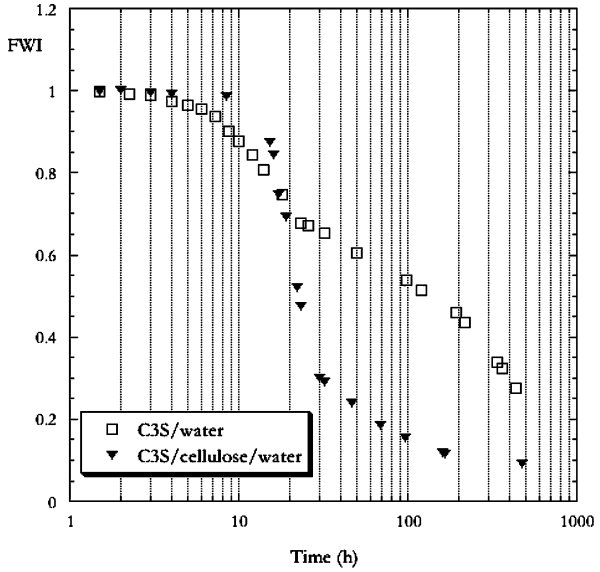

Figure 1. Comparison between the hydration process kinetics at 20 °C for C_3S/water and C_3S/water/MHEC pastes as obtained by differential scanning calorimetry.

Experimental longitudinal magnetization curves are compared with theoretical ones obtained by applying a spherical pore model, then, by minimizing the mean square root, the most probable pore size distribution function has been evaluated.[43,44]

Samples for calorimetric measurements have been prepared by the same procedure described for NMR experiments. Approximately 200 mg of C_3S has been mixed with 15 mg of previously prepared cellulose gel and with 65.5 mg of pure water. In this way a paste with a 0.4 water C_3S ratio by mass and with 0.27% MHEC on C_3S by weight has been produced. The paste (about 40 mg) was transferred in a stainless steel pan (diameter 7.4 mm, capacity 60 μL, from Perkin-Elmer) and sealed with the appropriate cover equipped with a neoprene O-ring. Each sample was maintained in a thermostatic bath at 20 °C. Differential scanning calorimetric measurements were performed on a Perkin-Elmer calorimeter DSC7, connected with a personal computer; data were elaborated with Pyris software for Windows, version 3.52. Measurements were repeated up to about 20 days after mixing.

Each measurement was carried out with the following temperature scan: from room temperature down to −30 °C at 40 °C/min, isothermal regime at −30 °C for 4 min, from −30 to −12 °C at 20 °C/min, from −12 to +14 °C at 4 °C/min.

The isothermal step at −30 °C was performed to ensure free water to freeze despite possible supercooling effects.

Each DSC curve showed a peak relative to water freezing and a peak due to its melting. From the enthalpy variation of the water melting, we calculate the free water index (FWI) according to the procedure reported in previous works.[11,19]

Results and Discussion

Figure 1 shows the comparison between the hydration kinetic obtained by DSC for C_3S cured at 20 °C with pure water and in the presence of MHEC. Both curves are characterized by

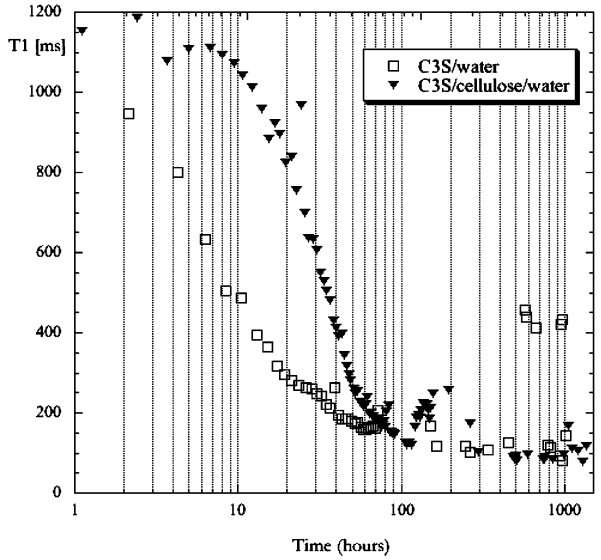

Figure 2. Spin−lattice relaxation time evolution for C_3S pastes hydrating in pure water and in the presence of MHEC.

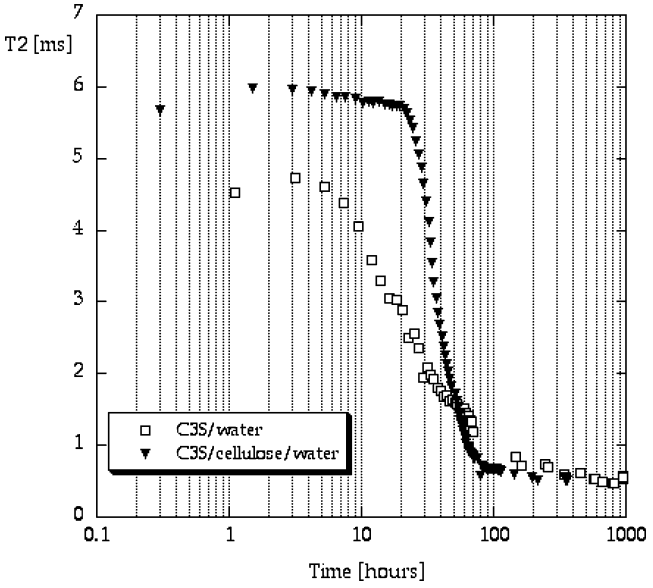

Figure 3. Spin−spin relaxation time evolution for C_3S pastes hydrating in pure water and in the presence of MHEC.

the well-known three stages of the hydration process: the induction period (lasting t_i), the acceleration stage, with a consistent decrease of free water index (FWI), and the diffusion period, marked by the slowing down of the hydration rate, which takes place at time above t_d. The acceleration stage for C_3S hydration starts after around 5 h in standard pastes and lasts approximately 20 h, on the other hand, t_i is 9 h in the presence of cellulose and last approximately until around 30 h. At first glance, the influence of MHEC on the hydration is evident: the presence of cellulose improves the efficiency of the hydration by increasing the amount of water involved in the hydration reaction. In fact, for the C_3S/water/MHEC paste, the acceleration period ends when only 20% of water remains nonreacted (FWI = 0.2), whereas for C_3S/water paste the nonreacted water is nearly 60%, meaning that in the presence of cellulose the C_3S is able to use most of the available water to complete the hydration reaction. It is worthwhile to recall that the water availability, as detected by the FWI, does not change for the binary system water/cellulose as evidenced by DSC analysis performed on this system for up to several days (data not reported). This effect can also be easily seen from the same FWI values found at the beginning of the hydration reaction for the binary (C_3S/water) and the ternary systems (C_3S/water/MHEC).

The measured NMR spin−lattice and spin−spin relaxation time values obtained from the pastes decrease with C_3S hardening, showing the progressive immobilization of water molecules during the hydration process.

Figures 2 and 3 show $T1$ and $T2$ magnetization decays. The spin−lattice relaxation time measured at the beginning of the hydration is approximately 1 s for C_3S/water paste and 1.1 s for C_3S/water/MHEC, while the spin−spin relaxation time is 4 ms for the C_3S/water system and 6 ms for the C_3S/water/MHEC one. The large difference between $T1$ and $T2$ values has been documented in literature for liquid phases in the presence of solid interfaces, as a consequence of a slow modulation of the dipolar relaxation of protons in the water molecules.[45]

The $T1$ relaxation time plot for the C_3S/water paste shows a sharp decrease without any induction period. The addition of MHEC modifies this behavior, increasing $T1$ values that are always longer at the correspondent hydration time and producing an increase of the induction period up to 6 h. Since $T1$ is related to the degree of freedom of water molecules in a constricted environment, it could be directly compared to the FWI obtained by the calorimetric approach, that is the amount of unreacted (or "unbound") water.

The decay of $T1$ of the C_3S/water paste and the corresponding FWI vs time curve are different in shape and, even though the shape of the $T1$ decay in the presence of MEHC closely resembles the DSC data plot, the induction is shorter in the former. This can be explained considering different populations of water molecules inside the paste. According to the most accepted model for cement hydration, water inside a hydrating paste can be classified into three phases: capillary water (free or bulk water), gel water (physically bound or surface water), and chemically bound water or nonevaporable water.[46−49] The calorimetric approach allows detection of the sum of the first two types of water, i.e., the evaporable amount of water present in the paste. It should be remembered that the liquid ^1H NMR technique is sensitive to the free (or capillary) water molecule signal, characterized by longer relaxation times, giving the interactions with the solid matrix and with the other water molecules. During the hydration process free water turns in gel water (water with some mobility restriction) and finally into bound water: as a consequence, the observed ^1H relaxation rate becomes progressively faster. From the previous considerations, the comparison between the results obtained with calorimetry and NMR can provide information about the mechanism of the progressive immobilization of water inside the paste.

The decrement of $T1$ value in the C_3S/water paste shows a change of slope at 20 h, and the curve approaches to a plateau around 200 ms: this value is reported in the literature as due to gel water.[47] From this result it can be inferred that all the residual water in the paste (around 60%, as evident from Figure 1) is gel water, while capillary water is no longer present. As at this hydration time the diffusion mechanism of hydration starts, it can be deduced that for the C_3S/water system this is correlated with the depletion of capillary water inside the paste.

MHEC modifies this behavior; the change in the slope of the $T1$ decrement occurs, in this case around 50 h, after which $T1$ approaches 200 ms, a value indicative of the presence of gel water inside the paste. In this case there is no correspondence between $T1$ decay and FWI decrement: in fact the diffusion period starts at 30 h. Thus, at this time the water available for

the reaction (20% of the total) behaves partly as gel water and partly as capillary water. Only after 50 h capillary water is not present any more, as indicated from $T1$ values around 200 ms.

These results indicate a greater efficiency in the hydration process for the C_3S/water/MHEC paste.

The dynamic of the water molecules, as observed from the behavior of $T1$ values, accounts for this effect, which becomes visible as a delay in the proton immobilization due to hydration. We can, therefore, infer that cellulose molecules act as a controlled-releasing agent for water during the C_3S phase hydration reaction.

To study the direct interaction of water with cellulose, relaxation times of the water proton in MHEC/water gel have been detected. The results obtained ($T1 = 1.23$ s and $T2 = 5.75$ ms) are indicative of very constrained water. Figure 3 shows the comparison between $T2$ behavior during hydration of the considered systems. The value of 4 ms, corresponding to the initial stage of the reaction in the C_3S/water paste, is reported in the literature as indicative of water constrained in capillary pores.[48] The initial plateau of the curve relative to C_3S/water/MHEC is around 6 ms, essentially the same as that of water entrapped in MHEC alone. This result supports the previous hypothesis about the strong interaction between the water and the cellulose molecules. It can be assumed that the supramolecular structure of MHEC/water system still remains almost unchanged inside the paste during the early stage of hydration. A similar behavior has been reported in the literature for a group of polymeric materials (covalently cross-linked poly-acrylates and copolymerized polyacrylamides−polyacrylates), indicated as super absorbent polymers (SAP), which absorb water and form macroinclusions inside the hydrating paste.[49]

Pore size distributions (PSD) of C_3S pastes in pure water and with MHEC added are reported in Figure 4. The PSD of the C_3S/water paste in the first step of the hydration is centered in the interval 120−140 μm. After 9 h the pore size dramatically shifts toward smaller values, in full accordance with previous results,[46,50,51] and continues to decrease until 19 h, when the distribution is almost entirely in the 0−20-μm interval. The system C_3S/water/MHEC presents a PSD centered in the interval 140−160 μm, in the first hours, and only a little shift can be observed in the first 19 h until 100−120 μm.

To visualize the morphological changes produced by MHEC on the C_3S hydration, the analysis of grain morphology by electron microscopy (SEM) was performed. The micrographs reported in Figure 5 A−L compare the two investigated systems, C_3S/water and C_3S/water/MHEC. The images (Figure 5A−D) show that until 12 h no relevant differences can be detected between the two systems. Figure 5E,G,I shows that the C_3S grains, which grow in a cellulose-free environment, are totally covered by fibril structures as expected for the setting process of C_3S. In contrast, in the images reported in Figure 5F,H,L, the fibrils of the typical CSH growing phase are not present, suggesting that cellulose affects the shape the hydrated CSH.

Conclusions

The use of chemical admixtures to ordinary cement pastes in order to improve the durability and strength for the new technological and architectural challenges has become a common use. Despite the proved effectiveness of these compounds, their effects on the cement microstructure are far from being fully clarified. NMR relaxation rate analysis allows the investigation of the evolution of the hydration process during the first steps of the cement paste setting. The results of the relaxation data elaboration can be compared with those obtained from other techniques, such as differential scanning calorimetry and images achieved by scanning electron microscopy, on a period lasting from the first hours of hydration until 12 days.

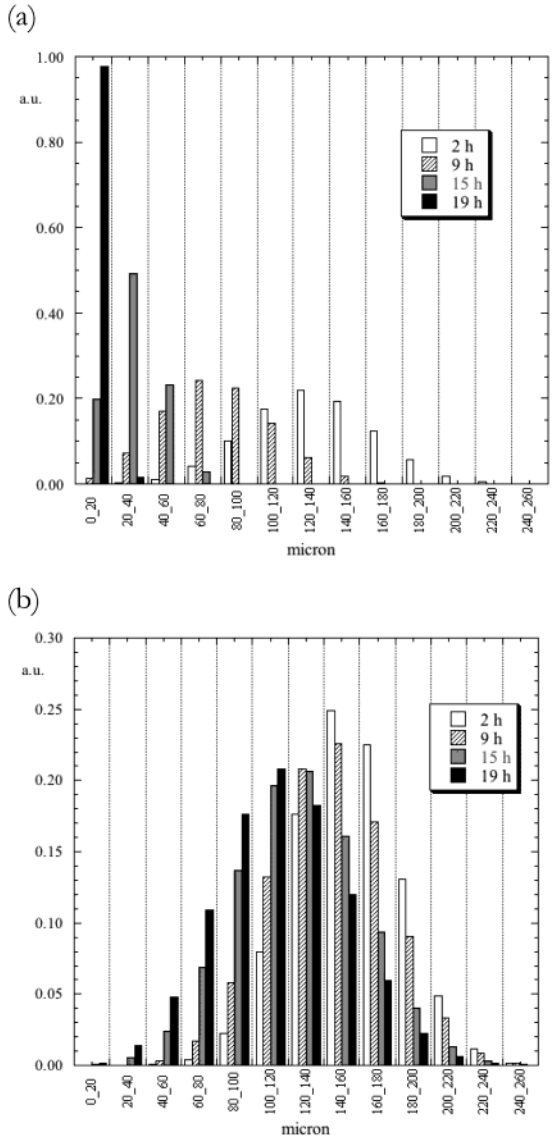

Figure 4. (a) Pore size distribution functions obtained for C_3S/water paste 2, 9, 15, and 19 h after mixing. (b) Pore size distribution functions obtained for C_3S/water/MHEC paste 2, 9, 15, and 19 h after mixing.

NMR relaxation time analysis accounts for the different water population according to the Powers model. In this sense, NMR provides additional information about the early stages of hydration and probes the contribution of capillary water (free water) and gel water (physically bound water), which are not differentiated by DSC.

All the experiments showed that cellulosic additives interact with water and strongly influence the hydration process. Relaxation time analysis and DSC demonstrates a mechanism of controlled-release of water mediated by MHEC. These findings open new perspectives on the modulation of cement features by adding appropriate additives and in the search of new additives for cement extrusion.

Acknowledgment. Thanks are due to Dr. L. Cassar, R. Alfani, G. Guerrini, and M. Biagini (CTG-Italcementi Group) for invaluable comments and discussions. Financial support from CTG-Italcementi Group, Ministero dell′Istruzione, Universita' e della Ricerca Scientifica (MIUR, grant PRIN-2003), and

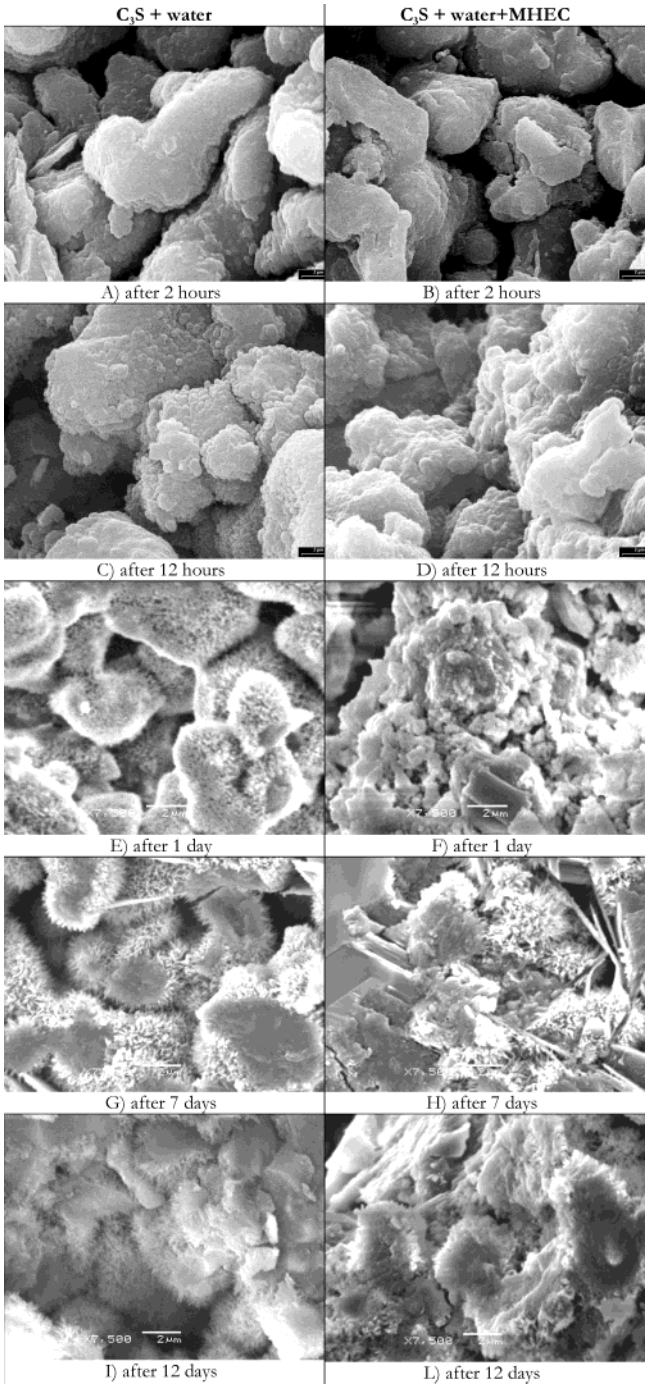

Figure 5. SEM images of pure C_3S samples and C_3S with added MHEC cellulose obtained at different setting times.

Consorzio Interuniversitario per lo Sviluppo dei Sistemi a Grande Interfase, CSGI, is gratefully acknowledged.

Appendix

K. R. Brownstein and C. E. Tarr developed a general model solely based on fluid bulk properties. They adopted the classical approach to the magnetization diffusion by Bloch and Torrey, where a magnetization density m(r,t) is defined according to the following differential equations:

$$D\nabla^2 m(r,t) = \frac{\partial m(r,t)}{\partial t} \tag{1}$$

$$(D\vec{n}\cdot\nabla m(r,t) + \rho m(r,t))|_s = 0 \tag{2}$$

where n is the normal vector to the surface, ρ is the surface relaxation, and D is the diffusion coefficient. Equation 1 establishes a simple pore volume condition, describing the magnetization transport by molecule diffusion. Equation 2 is a boundary condition on the pore surface accounting for the surface relaxation ρ. Strong dependence on the diffusion coefficient D is evident in both (1) and (2). Relaxation of the magnetization $M(t)$ derives from the following equation:

$$M(t) = m(r,t)V \tag{3}$$

with the starting condition

$$m(r,0) = \frac{M(0)}{V} \tag{4}$$

The pore size distribution can be obtained by comparing the experimental data describing the magnetization decay of water protons contained in porous samples with calculated data obtained according to different porous structures models. A suitable probability density function was chosen to describe the pore size distribution, where the pore radius is the positive variable. The method is based on the collection of longitudinal relaxation data using an inversion−recovery[27] experiment and on the comparison between experimental and theoretical longitudinal magnetization relaxation. The Brownstein and Tarr model was employed to obtain a theoretical description of the longitudinal magnetization decay as a function of the volume properties of the fluid. According to the Brownstein and Tarr model, pore geometry and relaxation intensity are bound by the coefficients of a sum of normal modes, depending on the diffusion coefficient D, on the surface-to-volume ratio, and on the pore size r. Surface-to-volume ratio values are obtained by the gas adsorption (BET) method.

Longitudinal magnetization decay is described by the following equation

$$M_z(t) = M_0\left(1 - 2\sum\nolimits_n I_n e^{-(t/T_n)}\right) \tag{5}$$

where the magnetization longitudinal component temporal evolution is reported as a function of a sum of normal modes whose coefficients are given for spherical geometries by

$$I_n = \frac{12[\sin(x_n) - x_n\cos(x_n)]^2}{x_n^3[2x_n - \sin(2x_n)]} \tag{6}$$

$$T_n = \frac{a^2}{Dx_n^2} \tag{7}$$

where the x_n's are the positive roots of

$$1 - x_n\cot(x_n) = \rho r/D \tag{8}$$

Depending on the value of the ratio $\rho r/D$, three different diffusive regimes can be identified:

$\rho r/D \ll 1$ is the fast diffusion regime; the time employed to diffuse to the surface is short compared to the surface relaxation, thus the observed decay is uniform all over the pore and all the spins are characterized by a single $T1$ value. This regime generates thus for a single pore a monoexponential magnetization decay and is characteristic of smallest pores where fluid rapidly diffuses experiencing to a limited extent the surface effects.

$1 < \rho r/D < 10$ is an intermediate regime where a deviation from the monoexponential decay is observable.

$\rho r/D \gg 10$ is the slow diffusion regime, where the time employed to diffuse on a distance r is long with respect to the surface relaxation. Thus fluid layers near the separation surface are clearly distinguishable from the inner ones and the relaxation is described by a linear superposition of monoexponential decays.

Basic assumptions for the model validity are listed below: bulk fluid intrinsic relaxation; surface relaxation for the fluid layers in contact with the pore walls; paramagnetic impurities acting as relaxation sinks; diffusion within the pore space with the coefficient D. Independently by the pore geometry, solutions are evaluated on the hypothesis that the effect on the relaxation due to the fluid interaction with the pore surface is uniform and quantifiable with parameter ρ.

The employed model is designed to simulate a porous medium with the following characteristics: pores are approximated as spheres with radius r; pore surfaces act as relaxation sinks, with constant intensity ρ; small throats connect pores. If pore connections are small enough, pores can be singly considered as if they were magnetically isolated, due to the enhanced relaxation in throats.

References and Notes

(1) Double, D. D.; Hellawell, A. *Nature* **1976**, *261*, 486−488.
(2) Double, D. D.; Hellawell, A. *Nature* **1977**, *237*, 82−90.
(3) Mishra, P. C.; Singh, V. K.; Narang, K. K.; Singh, N. K. *Mater. Sci. Eng. A* **2003**, *357*, 13−19.
(4) Saric-Coric, M.; Khayat, K. H.; Tagnit-hamou, A. *Cem. Concr. Res.* **2003**, *33*, 1999−2008.
(5) Lu, Z.; Zhou, X. *Cem. Concr. Res.* **2000**, *30*, 227−231.
(6) Silva, D. A.; John, V. M.; Ribeiro, J. L. D.; Roman, H. R. *Cem. Concr. Res.* **2001**, *31*, 1177−1184.
(7) Shao, Y.; Qiu, J.; Shah, S. P. *Cem. Concr. Res.* **2001**, *31*, 1153−1161.
(8) Klemm, A. J.; Klemm, P. *Buildings Environ.* **1997**, *32*, 195−198.
(9) Klemm, A. J.; Klemm, P. *Buildings Environ.* **1997**, *32*, 199−202.
(10) Baglioni, P.; Fratini, E.; Chen, S. H. *Appl. Phys. A* **2002**, *74*, S1178−S1181.
(11) Damasceni, A.; Dei, L.; Fratini, E.; Ridi, F.; Chen, S. H.; Baglioni, P. *J. Phys. Chem. B* **2002**, *106*, 11572−11578.
(12) Faraone, A.; Chen, S. H.; Fratini, E.; Baglioni, P.; Liu, L.; Brown, C. *Phys. Rev. E* **2002**, *65*, 040501−040501/040504.
(13) Faraone, A.; Fratini, E.; Baglioni, P.; Chen, S. H. *J. Phys. Chem., in press*.
(14) Fratini, E.; Chen, S. H.; Baglioni, P. *J. Phys. Chem. B* **2003**, *103*, 10 057−10 062.
(15) Fratini, E.; Chen, S. H.; Baglioni, P.; Bellissent-Funel, M. C. *Phys. Rev. E* **2001**, *64*, 1−4.
(16) Fratini, E.; Chen, S. H.; Baglioni, P.; Bellissent-Funel, M. C. *J. Phys. Chem. B* **2002**, *106*, 158−166.
(17) Fratini, E.; Chen, S. H.; Baglioni, P.; Cook, J. C.; Copley, J. R. D. *Phys. Rev. E* **2002**, *65*, 010 201.
(18) Fratini, E.; Faraone, A.; Baglioni, P.; Bellissent-Funel, M. C.; Chen, S. H. *Physica A* **2002**, *304* (1−2), 1−10.
(19) Ridi, F.; Dei, L.; Fratini, E.; Chen, S. H.; Baglioni, P. *J. Phys. Chem. B* **2003**, *107*, 1056−1061.
(20) Diamond, S. *Cem. Concr. Res.* **1999**, *29*, 1181−1188.
(21) Diamond, S. *Cem. Concr. Res.* **2000**, *30*, 1517−1525.
(22) Moro, F.; Bohni, H. *J. Colloid Interface Sci.* **2002**, *246*, 135−149.
(23) Bresson, B.; Zanni, H.; Masse, S.; Noik, C. *J. Mater. Sci.* **1997**, *32*, 4633−4639.
(24) Tzschichholz, F.; Herrmann, H. J.; Zanni, H. *Phys. Rev. E* **1996**, *53*, 2629−2637.
(25) Cory, D. G.; Garroway, A. N. *Magn. Reson. Med.* **1990**, *14*, 435−444.
(26) Kenyon, E. *Nucl. Geophys.* **1992**, *6*, 153−157.
(27) Kleinberg, R. L. *In Encyclopedia of Nuclear Magnetic Resonance*; Wiley: New York, 1996; Vol. 8.
(28) Song, Y.; Ryu, S.; Sen, P. N. *Nature* **2000**, *406*, 178−181.
(29) Davies, S.; Packer, K. J.; Roberts, D. R.; Zelaya, F. O. *Magn. Reson. Imaging* **1991**, *9*, 681−687.
(30) Hansen, E. W.; Gran, H. C.; Kvernberg, P. O.; Pederson, B. *J. Phys. Chem. B* **1997**, *101*, 9206−9214.
(31) Kleinberg, R. L. *Magn. Reson. Imaging* **1994**, *12*, 271−274.
(32) Kleinberg, R. L.; Kenyon, E.; Mitra, P. P. *J. Magn. Reson. A* **1994**, *108*, 206−214.
(33) Callaghan, P. T.; Coy, A.; MacGowan, D.; Packer, K. J.; Zelaya, F. O. *Nature* **1991**, *351*, 467−469.
(34) Hurlimann, M. D. *J. Magn. Reson.* **1998**, *131*, 232−240.
(35) Borgia, G. C.; Brown, R. J. S.; Fantazzini, P. *J. Appl. Phys.* **1996**, *79*, 3656−3664.
(36) Howard, J. J. *Magn. Reson. Imaging* **1994**, *12*, 197−200.
(37) Issa, B.; Mansfield, P. *Magn. Reson. Imaging* **1994**, *12*, 213−214.
(38) Alesiani, M.; Capuani, S.; Maraviglia, B.; Giorgi, R.; Baglioni, P. *Magn. Reson. Imaging* **2001**, *19*, 569.
(39) Brownstein, K. R.; Tarr, C. E. *Phys. Rev. A* **1979**, *19*, 2446−2453.
(40) Callaghan, P. T. *Principles of Nuclear Magnetic Resonance Microscopy*; Clarendon Press: Oxford, 1991.
(41) Borgia, G. C.; Brown, R. J. S.; Fantazzini, P. *J. Magn. Reson.* **1998**, *132*, 65−77.
(42) Borgia, G. C.; Brown, R. J. S.; Fantazzini, P. *J. Appl. Phys.* **1997**, *82*, 4197−4203.
(43) Alesiani, M.; Capuani, S.; Maraviglia, B.; Giorgi, R.; Baglioni, P. *Appl. Magn. Reson.* **2002**, *23*, 63−73.
(44) Appolonia, L.; Borgia, G. C.; Bortolotti, V.; Brown, R. J. S.; Fantazzini, P.; Rezzaro, G. *Magn. Reson. Imaging* **2001**, *19*, 509−512.
(45) Delville, A.; Letellier, M. *Langmuir* **1995**, *11*, 1361−1367.
(46) Taylor, H. F. W. *Cement Chemistry*; 2nd ed.; Thomas Telford: London, 1997.
(47) Plassais, A.; Pomiès, M. P.; Lequeux, N.; Boch, P.; Korb, J. P. *Magn. Reson. Imaging* **2001**, *19*, 493−495.
(48) Greener, J.; Peemoeller, H.; Choi, C.; Holly, R.; Reardon, E. J.; Hansson, C. M.; Pintar, M. M. *J. Am. Ceram. Soc.* **2000**, *83*, 623−627.
(49) Jensen, O. M.; Hansen, P. F. *Cem. Concr. Res.* **2001**, *31*, 647−654.
(50) Odler, I.; Chen, Y. *Cem. Concr. Res.* **1995**, *25*, 919−923.
(51) Skalny, J.; Odler, I. *J. Colloid Interface Sci.* **1972**, *40*, 199−205.